Published: *J. Geophys. Res. Vol. 105, No. A8*, p. 18,729

Comprehensive particle and field observations of magnetic storms at different local times from the CRRES spacecraft

A. Korth,[1] R. H. W. Friedel,[1,2] C. G. Mouikis,[1,3] J. F. Fennell,[4]
J. R. Wygant,[5] and H. Korth [2]

Abstract.

The response of ring current intensification to three magnetic storms sampled at dawn, midnight, and dusk is investigated. We use a comprehensive set of data from the CRRES satellite, using plasma, energetic particle (ion composition), electric field, and magnetic field data, which is ideal for investigating the interrelationship between the ring current strength as measured by D_{st}, the particle (current carriers) in the outer radiation belt, their effects on the global magnetic field, and the convection effects caused by large dawn-dusk electric fields. This yields a comprehensive and self-consistent picture of storm time radiation belt formation based entirely on data. At all local times investigated strong, stretching (flattening) of the magnetic field down to $L < 4$ is observed during the storm main phase, showing that this field line stretching is not limited to midnight. Ring current ions above 100 keV are shown to form a partial ring current during the main phase as they are only sampled at dawn during the recovery phase when the electric field vanishes. Comparing this feature to Kp-dependent models of the proton Alfvén layer shows that dawn is only accessible to these ions after the main phase. Ionospheric origin ions (O^+) follow dynamics very similar to those of H^+, indicating a source in the plasma sheet. Solar wind ions (He^{++}) are controlled by their solar wind source and have immediate access during the main phase. He^+, which is generated in the ionosphere as well by charge exchange, has behavior similar to that of as O^+ and H^+. In contrast to the current view, plasma sheet ions in the energy range from 5 to 28 keV contribute significantly in the energy density of the ring current during the storm main phase.

1. Introduction

Magnetic storms, the ring current, and their effects as measured on the ground through the D_{st} index are amongst the oldest topics in magnetospheric physics. D_{st}, in particular, is widely and sometimes indiscriminately used as an input parameter to models or a sorting parameter for statistical studies; this often ignores the fact that at best such a global index provides an average indication of the ring current dynamics.

We show here in detail the relation between the D_{st} index and in situ measurements of both the particle and field measurements that contribute to this index. Having assembled a comprehensive set of particle and field measurements for the CRRES mission allows us to present "the full picture" of ring current formation during storm times, based entirely on data.

As it is impossible to cover all local times and radii with a single spacecraft, we present here three storms measured at three different local times of the CRRES apogee. In this way we can highlight the differences and commonalities of the storm time dynamics observed at various points in the magnetosphere. We cannot cover dayside magnetic storms as the CRRES mission terminated before apogee reached noon.

The concept of two different storm time ring current systems, a symmetric one and an asymmetric one, has been accepted for some time [*Kawasaki and Akasofu*, 1971]. This topic has been revisited in detail from

[1]Max-Planck-Institut für Aeronomie, Katlenburg-Lindau, Germany.
[2]Los Alamos National Laboratory, Los Alamos, New Mexico.
[3]Space Science Department, University of New Hampshire, Durham, New Hampshire.
[4]The Aerospace Corporation, El Segundo, California.
[5]School of Physics and Astronomy, University of Minnesota, Minneapolis.

a ground-based magnetic field measurements point of view by *Grafe* [1999], who concludes that even in quiet times there is no such thing as a "symmetric" ring current, that in fact it is always "weakly asymmetric". This asymmetry increases during storms and recovers rather fast to its weakly asymmetric quiet time state. *Grafe* also demonstrated that the degree of asymmetry reached during storms depends on how powerful the storm is. While we do not have the statistical coverage here to corroborate an always "weakly asymmetric" ring current, we can demonstrate from a particle point of view that storm time asymmetries exist, and we can also show where they exist. Using the concept of Alfv́en layers allows us at least to explain the storm time asymmetries observed by *Grafe* solely on the basis of inner magnetospheric access considerations for ring current ions. D_{st} is supposed to be corrected for any asymmetric components. We can show here in the data which ions have access to the dawnside during the storm main phase, demonstrating that a partial ring current exists during this phase, which is not reflected in D_{st}. While this is a feature that has been expected by many authors, we can here demonstrate it conclusively with data.

In order to address the role of minor species ions in the formation and decay of the ring current, we use ion composition measurements. Ionospheric oxygen, in particular, has received much attention as a possible major contributor to the ring current density at storm onset [*Daglis*, 1997], although the exact access mechanism for these ions remains unclear. We present evidence here that this source lies primarily in the plasma sheet, however, we do not speculate on how these ions are extracted from the ionosphere in the first place.

We do not investigate the role of substorms as a contribution to the ring current in this paper, even though substorms were present during the onset and recovery phase of all three storms presented here. This topic has been addressed by *Korth et al.* [1998]. We concentrate here on the role of ion species and the access that ions have to various parts of the inner magnetosphere during storms. The remainder of this paper is organized in the following way: Section 2 describes briefly the CRRES mission and the instrumentation used. Section 3 gives a common description of the data plots used for each storm before dealing with each storm in detail. The discussion of the results follows in sections 4 and 5, dealing with the magnetospheric access and storm composition issues.

2. Mission and Instrumentation

This investigation uses particle, electric, and magnetic field measurements from the Combined Release and Radiation Effects Satellite (CRRES), which had an elliptical, 18.1^o inclination orbit with a period of 9 hours 52 min. CRRES covered the regions up to $L = 8$, giving an L profile twice an orbit, at magnetic latitudes mostly within 20^o of the magnetic equator. The orbit apogee precessed from the prenoon sector at launch (August 1990) to the early dusk sector at the end of the mission (October 1991).

On CRRES the Medium Electrons B spectrometer (MEB) [*Korth et al.*, 1992] covers electrons from 21 to 285 keV and total ions (no composition) from 37 keV to 3.2 MeV. The Magnetospheric Ion Composition Spectrometer (MICS) [*Wilken et al.*, 1992] measures the mass, energy, and the charge of particles with energies of 1- 430 keV per charge. The Low Energy Plasma Analyzer (LEPA) [*Hardy et al.*, 1993] covers electrons and ions (no composition) in either the energy range 120 eV to 20 keV or 160 eV to 28 keV. The electric field probe [*Wygant et al.*, 1992] consists of two pairs of orthogonal sensors with tip-to-tip separations of $\sim 100\ m$ in the spin plane of the spacecraft. The sensitivity is better than $0.1\ mV/m$ and the dynamic range is of the order of $1000\ mV/m$. The fluxgate magnetometer [*Singer et al.*, 1992] instrument is located on a 6.1 m boom. Magnetic field data are presented in the VDH coordinate system, where H is anti-parallel to the magnetic dipole axis, V is radially outward in the magnetic equatorial plane, and D is eastward, completing the orthogonal right-handed coordinate system.

3. Observations

The data presented in this paper are L-sorted plots versus time of the type used by *Friedel and Korth* [1995] and *Korth and Friedel* [1997]. For each half orbit (4 hours 55 min) the data are averaged over bins $0.2\ L$ wide which correspond to one vertical stripe in the plots. L values are from the Olson-Pfitzer 1977 quiet model, which is tilt-dependent and fits quiet conditions (Kp = 0–1) [*Olson and Pfitzer*, 1977]. The model is valid from 2.5 to 15 R_E. This model was shown to provide the best overall fit to the CRRES magnetic field data [*Jordan et al.*, 1992].

In Plates 1 – 3 the plots are numbered from top. We explain here each plot in turn:

Plots 1 and 2 show data from the magnetic field instrument. We subtract the Olson-Pfitzer 1977 quiet

model from the measured parameters so that the difference between the disturbed and quiet conditions can be seen. Plot 1 gives the angle between the magnetic H and V components and is a measure of the stretching of the field lines compared to the dipole field. Positive (yellow to red) values indicate a stretched field topography. Plot 2 gives the residual magnetic field H component, which for near-equatorial orbits responds directly to equatorial current systems such as the ring current. Negative values (light blue to dark blue) give an indication of the depression of the H component due to local current systems including the partial or symmetric ring current.
Deviations from the model field are also a direct indicator of the fidelity of the L values used. In the plots presented here a static L value from the quiet field was used. During disturbed (stretched) times as indicated in plots 1 and 2, the model overestimates L, as the satellite actually sits on lower, stretched field lines. The amount of error increases with L and with the "depth" to which field line stretching penetrates. This effect makes labeling the data by L somewhat unreliable during the onset phase of a storm. Typically, stretching is seen at higher L during the recovery phase (near geostationary orbit), and the L values near the peak of the ring current are not affected.

Plot 3 represents one channel from the spherical or cylindrical probe of the electric field instrument. It shows the variation of the dawn-dusk (E_y) electric field component in a frame of reference corotating with the Earth. The data here have been corrected for the spacecraft motion and the corotation speed of the Earth and thus represent the residual dawn/dusk field only [*Wygant et al.*, 1998]. Short-lived, localized enhancements are mainly due to local transient electric fields caused by substorms, while the more contiguous, longer-duration enhancements are associated with global, storm time dawn-dusk fields caused by enhanced convection.

Plots $4-11$ display the variation of the energy density of the ion species O^+, He^{++}, He^+, and H^+, respectively, as measured from the ion composition spectrometer MICS. For each species the data are integrated over two similar energy ranges. These ranges have been chosen to demonstrate the difference in storm time behavior of these populations in terms of global inner magnetospheric access. Both ranges taken together are representative of the main part of the ring current density ($\sim$ 30 to 160 keV), and are used here to show the relative importance of ion composition in contributing to the ring current.

Plot 12 shows the variation of the energy density of all ions as determined from the LEPA instrument over an integrated energy range of $\sim$ 5 to 30 keV. This indicates the contribution of plasma sheet particles to the ring current.

Plot 13 shows the D_{st} index as a measure of the ring current during magnetic storms. In magnetic storm we commonly identify three phases: the initial phase, the main phase, and the recovery phase. These phases can be identified using the D_{st} index. During the initial phase, the interplanetary magnetic field (IMF) is northward, and the horizontal magnetic field component increases owing to a compression and distortion of the dayside magnetosphere (enhanced solar wind pressure). This can last several hours but is not a feature of all storms. During the main phase strong earthward convection exists, the ring current grows, and the horizontal magnetic field component decreases. The IMF is usually southward. Finally, in the recovery phase the IMF weakens or turns northward, and the ring current stops growing. The horizontal magnetic field component increases slowly while the ring current ions decay. This recovery can take several days. The black vertical dashed lines in Plates 1–3 mark the beginning of the activity while the solid lines mark the start of the recovery phase. The dashed horizontal lines indicate zero D_{st}.

Care needs to be taken in the interpretation of these overview-type figures. Individual vertical stripes in Plates 1–3 represent data from one CRRES half orbit, and are assigned a time corresponding to the middle time for that half orbit. Timing accuracy is inherently limited to 4 hours 55 min. As there is a further directional bias, as each stripe represents data from an inbound or outbound pass, features at a given L value can be "missed" and only show up in the next stripe.

3.1. Dawnside Magnetic Storm (October 9–10, 1990)

An isolated storm, which occurred when CRRES apogee was near 0500 magnetic local time (MLT), with a minimum D_{st} value of -133 nT, is shown in Plate 1 over a time period of 9 days. The (B_z, ΔT) trigger of -8.7 nT for $\sim$ 10 hours (data were taken from IMP 8 and are not shown) indicates an intense storm [*Gonzalez et al.*, 1994]. Northward turning of B_z (vertical solid line) initiates the recovery phase.

With the beginning of the main phase of the storm a stretching of the magnetic field (plot 1) is observed. The stretching is propagating to lower L values and reaches in this event $L = 4 - 4.5$ at the end of the

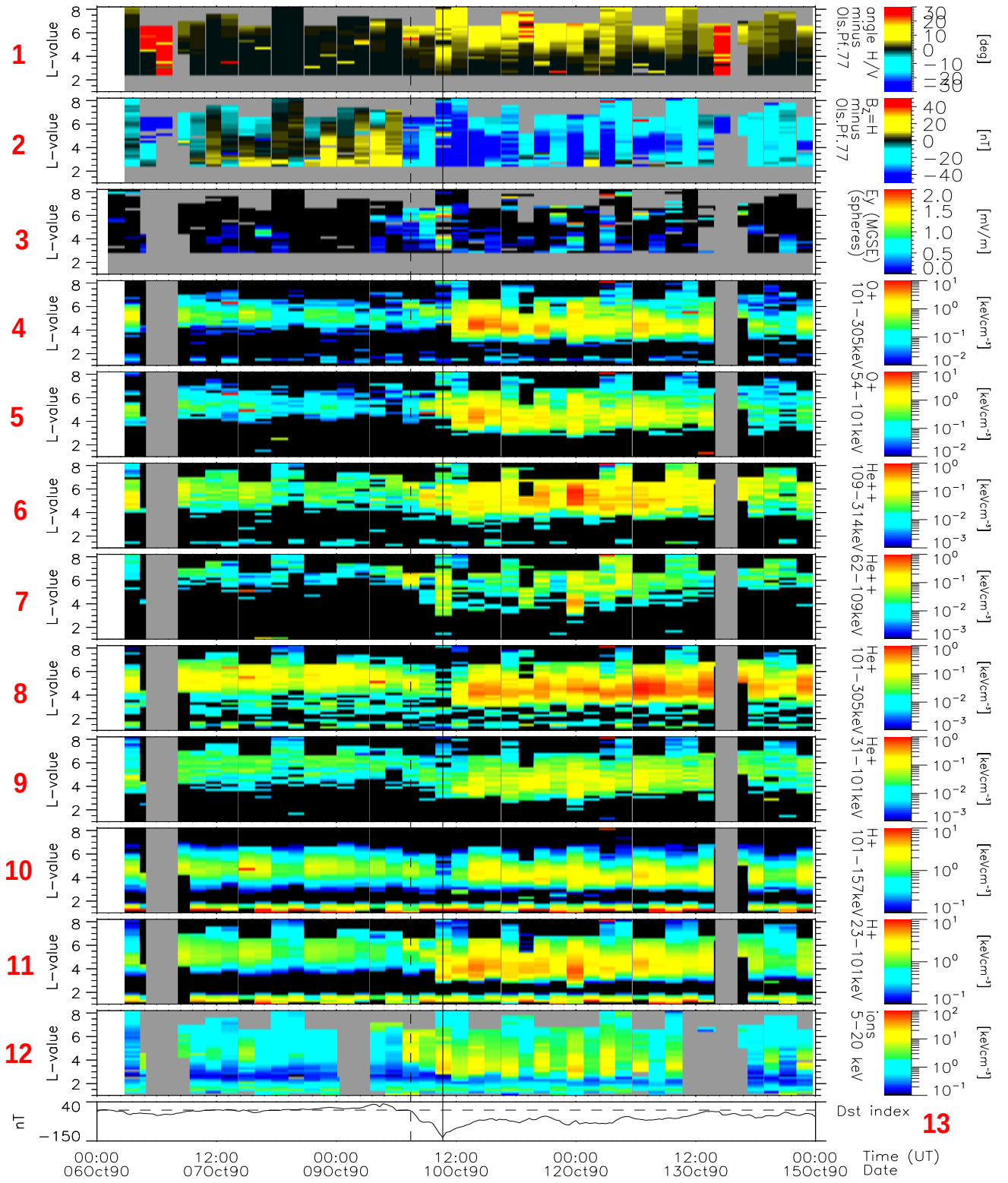

Plate 1. Data for the dawn storm. See text for details.

main phase. At the same time the H component is reduced in magnitude at all L ranges (plot 2), which is indicative of an increased equatorial ring current. During the storm main phase a large electric field component E_y is present at CRRES and can be seen to penetrate deeper and deeper into the magnetosphere on subsequent half orbits (plot 3). The maximum field strength down to $L = 3$ is reached at the end of the main phase. These measurements are local and indicate the dawn-dusk component of the electric field at CRRES only, and these measurementsare are thus only a proxy for the large-scale convection electric fields existing farther down tail. The ring current during the main phase is due to plasma sheet ions (plot 12) only, as the normal ring current energies shown in plots 10 and 11 are not present yet at this time. Plot 12 shows all ions independent of species, whereas the later arrival of higher-energy ions is also seen by O^+ (plots 4 and 5) and He^+ (plots 8 and 9). The break in the energy range used between the higher-ion-energy plots and plot 12 was chosen to demonstrate this feature. A full explanation of this energy-dependent access of ions is given in section 4. Ionospheric ions (O^+ and He^+) have a response very similar to that of protons, while He^{++} ions which are of solar wind origin not only appear during the main phase but also have their highest intensity in the recovery phase 1 R_E farther out compared to the other ion species. The ion composition is further examined in section 5.

The beginning of the recovery phase is clearly marked by the turning off of the electric field, which stops the access of fresh plasma sheet ions. These ions have reached their lowest L at this point. This also now allows the more energetic ring current ions to have access to the morningside and to establish complete drift orbits (see section 4). The stretched and depressed magnetic field also starts recovering with recovery fastest at low L. The position of the maximum depressed field is also a good indicator of the ring current position and agrees well with the position of the maximum energy density of the ring current ions during the recovery phase. The "sudden" access of energetic ring current ions to the morningside in the recovery phase is due to the sampling by CRRES, which sees the particles "appearing" at a large L range during one half orbit, unable to resolve any timing information below 5 hours.

3.2. Midnight Magnetic Storm (February 02–03, 1991)

A second magnetic storm occurring when CRRES apogee was near 2330 MLT (Plate 2) is shown over a time period of 9 days. The minimum D_{st} is -78 nT. The (B_z, ΔT) trigger of -10 nT for $\sim$ 3 hours (data were taken from IMP 8 and are not shown) indicates a moderate storm [*Gonzalez et al.*, 1994]. Northward turning of B_z (vertical solid line) initiates the recovery phase.

This storm exhibits some ring current enhancement prior to the onset of the main phase. A small dawn-dusk electric field is observed, the field is stretched beyond $L = 5.5$, and the magnetic field H component is depressed. Particles of all species are convected to L values beyond $L = 5$ except high-energy O^+ (above 113 keV).

With the beginning of the main phase an enhanced dawn-dusk electric field is observed, the magnetic field is stretched to lower L values, the Hcomponent is depressed further, and the particles intensify immediately and are brought to lower L values. In the recovery phase of the storm there is a general decay of particles. Lower energies decay faster, and their maximum moves to larger L. Ring current particles of H^+, He^+, and O^+ above 100 keV are fairly stable and decay much more slowly. Their maximum is at $L = 4.5$ whereas the maximum of He^{++} is $\sim$ 1 R_E farther out. In comparison to the magnetic storm on the dawnside of the magnetosphere we notice that CRRES sees at midnight the full convection paths of the ring current ions of all species and an intensification right at the onset of the storm (see section 4 for details).

3.3. Duskside Magnetic Storm (July 09–10, 1991)

Two further magnetic storms occurring when CRRES apogee was near 1730 MLT (Plate 3) are displayed over a time period of 13 days. For the interpretation we will use the first magnetic storm on July 09–10, 1991. The minimum D_{st} is -194 nT. During the second storm ($D_{st} = -183$ nT) the spacecraft was at higher geomagnetic latitude and spent quite some time during the storm main phase in the lobes of the magnetosphere. Therefore the ring current data are more difficult to interpret.

The (B_z, ΔT) trigger stayed negative for $\sim$ 11 hours with a minimum B_z value of about -40 nT (data were taken from IMP 8 and are not shown) and indicates an intense storm [*Gonzalez et al.*, 1994]. Northward turning of B_z (vertical solid line) initiates the recovery phase.

Magnetic field data in plot 1 and 2 are contaminated by bad data before and during the main phase of the

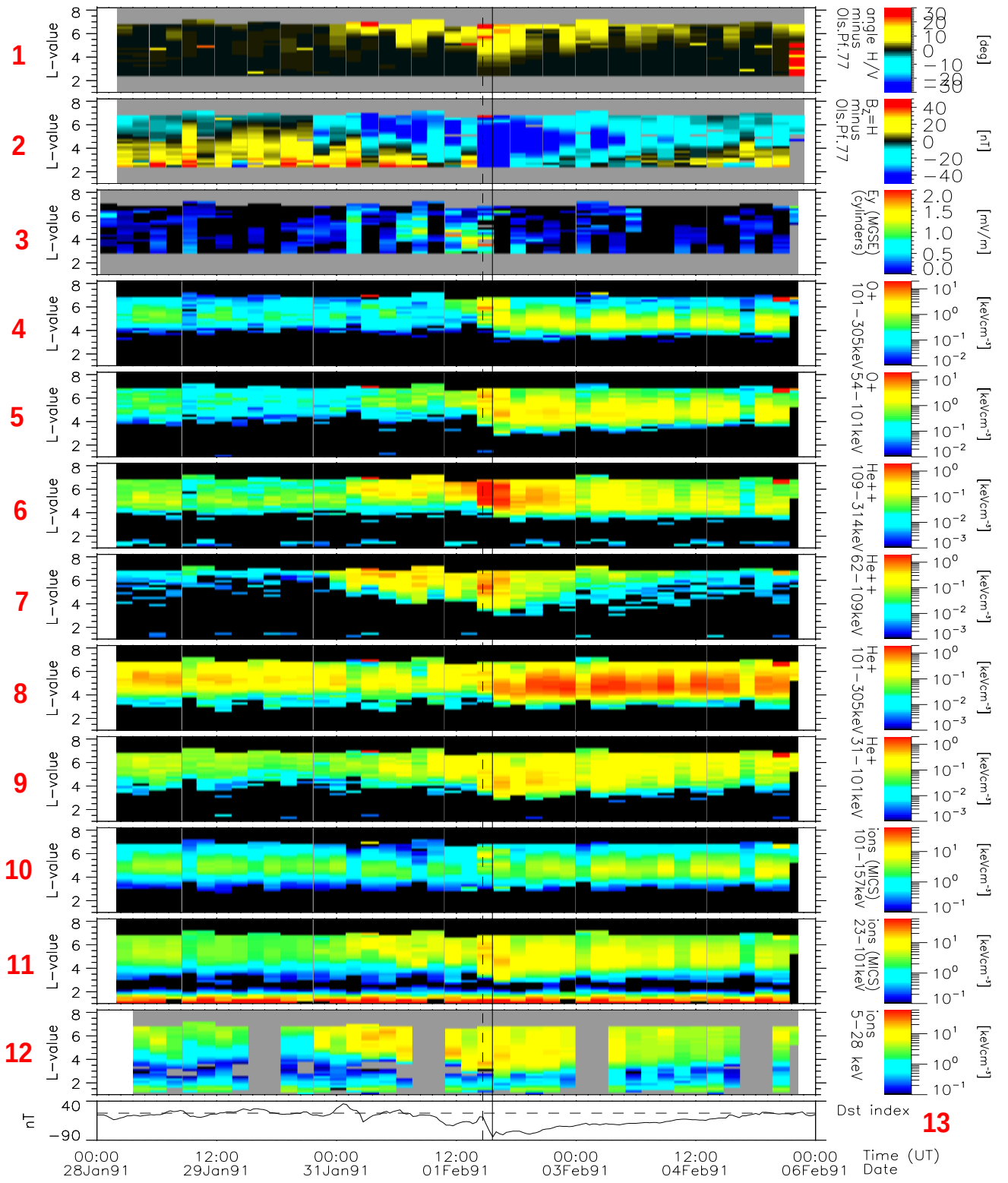

Plate 2. Data for the midnight storm. See text for details.

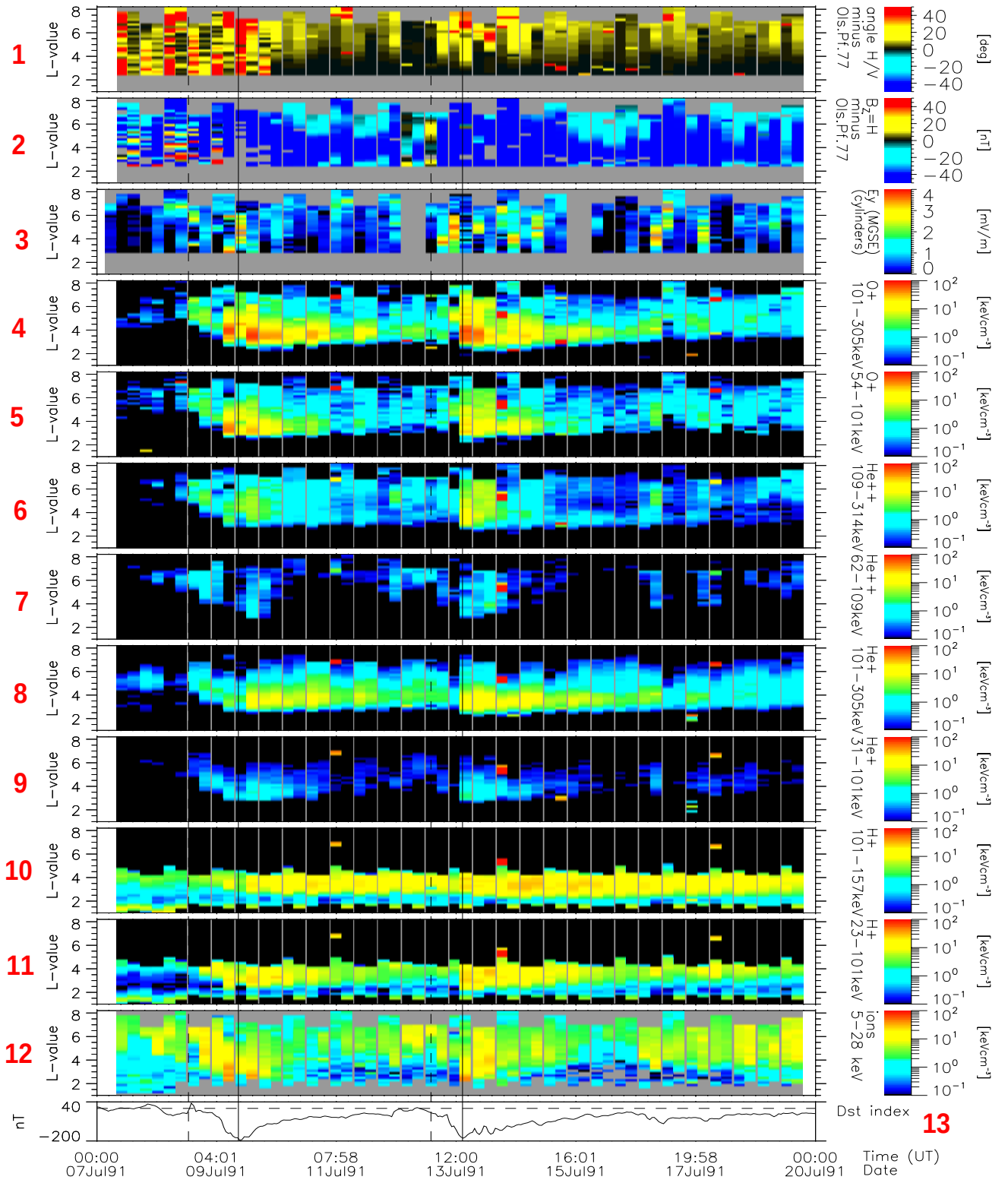

Plate 3. Data for the dusk storm. See text for details.

first storm. However, a clear stretching of the magnetic field is observed during the recovery phase of the storm. During this July 1991 storm, which is the strongest of the three storms examined here, the dawn-dusk electric field not only penetrates to low L values during the main phase but is stronger between $L = 2.7$ and $L = 6.0$ (up to 4 mV/m) than it is at higher L values. This is a robust feature of the radial structure of the electric field during the stongest magnetic storms observed during the CRRES mission [*Wygant et al.*, 1998; *Rowland and Wygant*, 1998]. This suggests that a major portion of the convection electric field has migrated to the inner magnetosphere during these times. In the recovery phase a weak electric field is observed for a few days.

Low-energy ions ($5 - 28$ keV) as well as energetic ions ($30 - 157$ keV) in plots $4 - 12$ are observed simultaneously at dusk with the beginning of the storm main phase (see section 4 for details). This is also true for all ion species. These ions are convected during the main phase by the electric field from geosynchronous orbit to as low as $L = 2.5$. In the storm recovery phase the ions decay, and the ring current maximum is moving about an Earth radius outward to $L = 4.5$.

4. Storm Proton Access at Different MLT

The previous three examples point out some marked differences between the storm time response sampled at dawn and that at midnight and dusk, mainly during the storm main phase. The longer-term behavior shows strong commonality at all local times:
1. Strong stretching of the magnetic field is observed during onset and recovery, which is in good temporal and spatial correlation with the main ring current population.
2. The storm main phase is marked by strong dawn-dusk electric fields which penetrate deep into the magnetosphere, and the start of recovery is clearly marked by a turning off of the electric field (northward turning of the IMF B_Z, not shown here).
3. Location and strength of the recovery phase radiation belt correlate well with the ring current position and field line stretching as measured by the magnetic field data.

The differences in the storm main phase at dawn are primarily the delayed access of > 30 keV ions; they only appear with the beginning of the recovery phase. There are several possibilities that could prevent access of ring current ions to the dawnside during the main phase:
1. The first possibility is magnetopause shadowing which is caused by a large compression of the magnetopause down to low L, preventing particles from completing a full drift.
2. The second possibility are strong local loss processes. At geosynchronous orbit the bulge of the plasmasphere is seen once per day per satellite in the dusk sector of local time [*Borovsky et al.*, 1998]. During high geomagnetic activity, plasmaspheric material is being stripped off of the outer plasmasphere and removed from the magnetosphere at the dayside magnetopause. MHD calculations of the equatorial cross section of the plasmasphere [*Kurita and Hayakawa*, 1985] during increasing magnetic activity show narrow flow channels. Observations suggest that some cold plasma of the plasmasphere is indeed dragged along and carried out to the magnetopause during periods of enhanced disturbance activity [*Grebowsky*, 1971; *Carpenter et al.*, 1993; *Elphic et al.*, 1996; *Borovsky et al.*, 1998]. The hot ions or ring current ions interact with the cold plasma. Strong cyclotron wave-particle interactions can occur in the ring current region and can lead to strong pitch angle diffusion and highly localized precipitation of ions into the ionosphere.
3. The third possibility is no drift path access. During the strong cross-tail electric fields in the main phase a substantial part of the source population of the ring current (plasma sheet ions) is on open drift paths which do not have access to dawn and only become trapped in the recovery phase.

We have found here that our observations can be adequately explained by possibility 3 above, in terms of the Alfvén Layer concept (trapping boundary). It has long been understood that the basic mechanism of trapping new populations into the ring current occurs with the following steps [*Williams*, 1987]:
(1) Strong dawn-dusk electric fields,
(2) enhanced convection,
(3) shrinking Alfvén boundary,
(4) enhanced convection on open drift paths to lower L,
(5) electric field vanishes,
(6) Alfvén boundary moves to higher L,
(7) previously open drift paths become trapped, and
(8) enhanced radiation belt population.

While the overall storm time features are well described by the above procedure, the local time variation has often been ignored or has not been comprehensively measured such as was possible with CRRES. The shape of the Alfvén boundary is not symmetric and a function of both the convection electric field strength and particle energy. The Alfvén boundary results shown here are taken from model calculations by *Korth et al.* [1999].

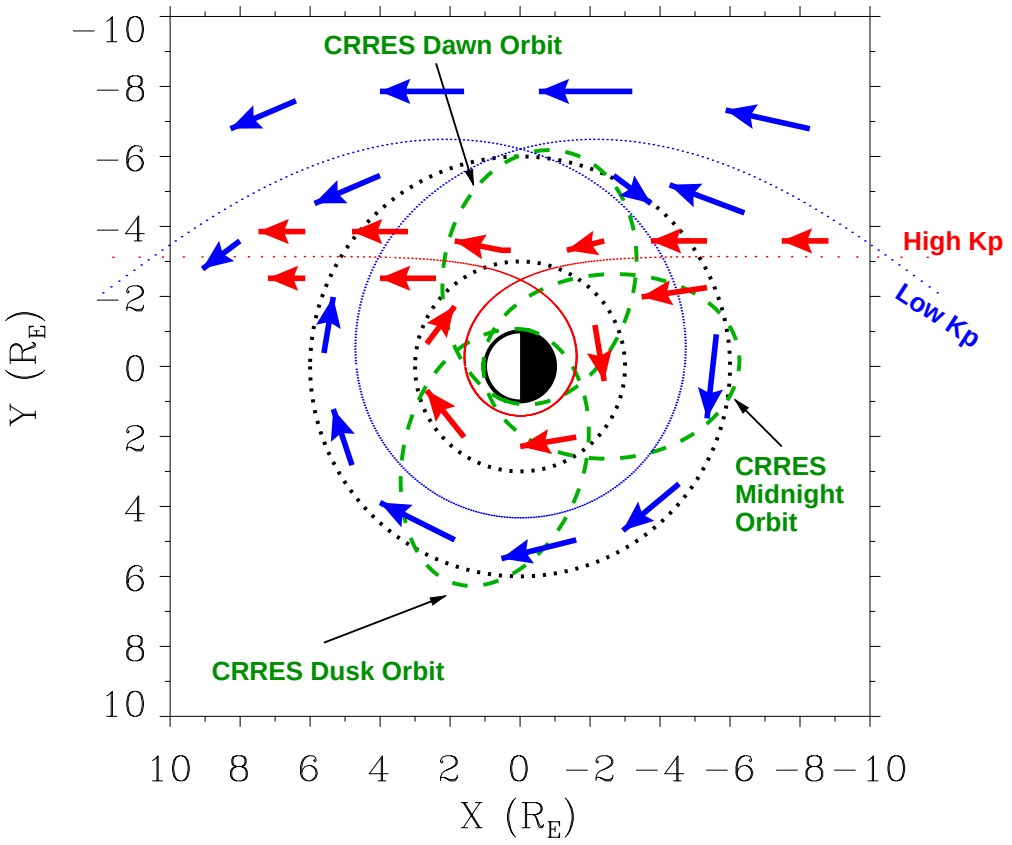

Plate 4. The 5 keV proton (at $L = 6.6$) Alfvén boundaries and convection paths for low Kp (low cross-tail electric field) in blue and for high Kp (high cross-tail electric field) in red. Also shown are three representative CRRES orbits for the storms observed at the different MLTs in green and black dashed reference circles at 3 and 6 R_E.

The calculations are for equatorially mirroring particles in a dipole field. The electric field is a superposition of a shielded cross tail and a corotational electric field. The cross-tail electric field is parameterized by Kp using the empirical relationship established by *Gussenhoven et al.* [1981, 1983].

In Plate 4 we show the Alfvén boundary for 5 keV protons, which is representative for the data in plot 12 of Plates 1–3. Representative CRRES orbits for the dawn, midnight, and dusk storms are plotted in green.

We see that during the storm main phase (high Kp and high cross-tail electric field) the trapped region inside the red Alfvén boundary is very compressed. However, these lower-energy ions continue to have access to the CRRES orbit at dawn from the enhanced sunward convection across the dawnside, which for high Kp can be below 3 R_E as shown in Plate 4. So these particles can reach CRRES orbits at the dawn side immediately upon the beginning of the storm main phase and are seen as soon as the enhanced electric field (plot 3, Plate 1) is observed at CRRES. At midnight and dusk these particles have access by drifting around the duskside, and are also seen immediately with the beginning of the storm main phase.

During the recovery phase, as soon as the electric field vanishes, the Alfvén boundary moves out to the curve shown in blue for low Kp in Plate 4. The whole inner region up to ~ 5 R_E ends up inside the Alfvén boundary for these energies, and that population becomes trapped. This can be clearly seen in plot 12 of Plate 1, where the peak in the population is seen to be near $L = 4$ (note that at these low L values $L \sim R_E$).

We investigate the access for 30 keV protons in a similar manner in Plate 5, which is analogous to Plate 4. This energy is representative for the data in plot 11 of Plates 1–3.

The Alfvén boundaries for higher-energy particles move farther out in general. In this case the asymmetric shape of the Alfvén boundaries is important. During

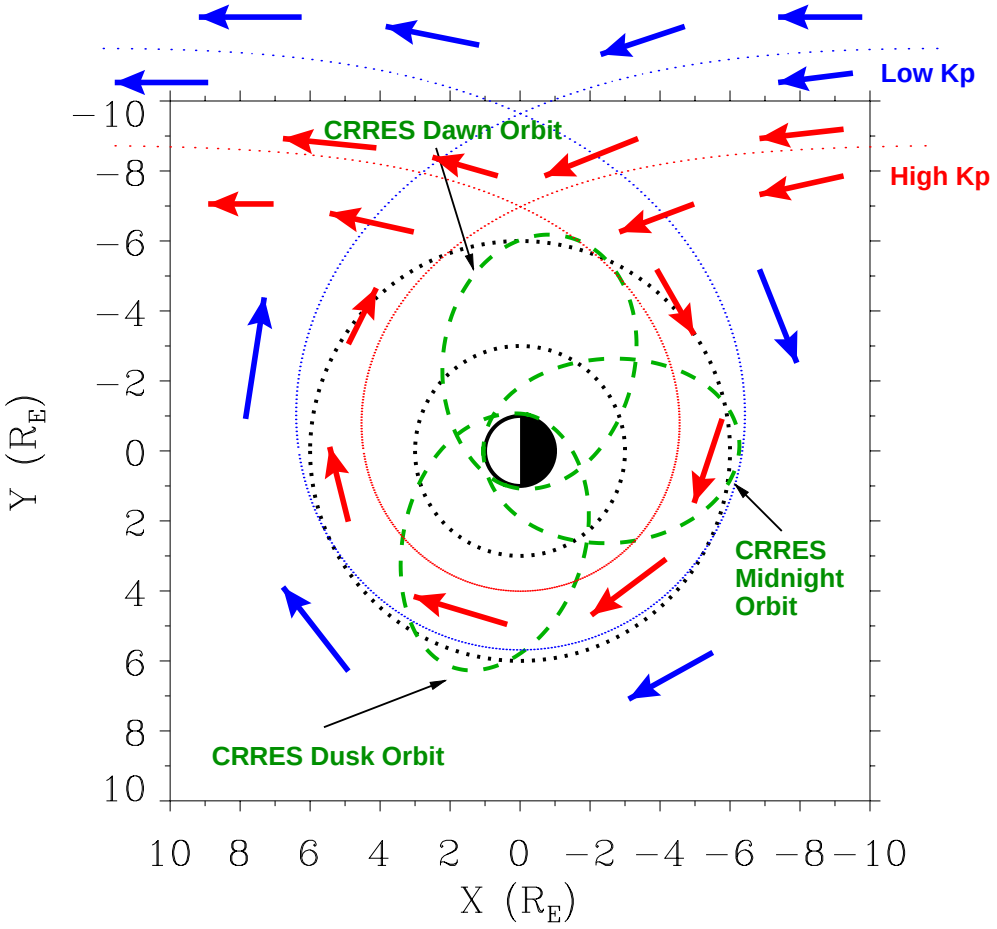

Plate 5. The 30 keV proton (at $L = 6.6$) Alfvén boundaries and convection paths for low Kp (low cross-tail electric field) in blue and for high Kp (high cross-tail electric field) in red. Also shown are three representative CRRES orbits for the storms observed at the different MLTs in green and black dashed reference circles at 3 and 6 R_E.

storm onset (high Kp and high cross-tail electric field) these higher energies do not have access to the dawnside, because of the bulge in the Alfvén boundaries at 0600 MLT, and most of the CRRES orbit lies within previously closed drift paths. Newly convected particles from the tail do have access to as low as 4 R_E on both the midnight-side and dusk-side during this period, and these particles can be seen there much earlier than they can at dawn.

During the recovery phase, as soon as the cross-tail electric field vanishes, the Alfvén boundary moves out to the curve shown in blue for low Kp in Plate 5. Now the population which had been convecting around dusk (red arrows) becomes trapped and has access to the dawnside. Thus these energies only appear at the dawn CRRES orbits at the beginning of the recovery phase.

In the above discussion we have ignored any dynamic effects of the filling or emptying of drift shells as they become closed or open. Ring current ions take a finite time to occupy a new drift shell completely and also take a finite time to be lost from a drift shell once it is no longer closed. These transit periods are of the order of the particle drift period, which for the energy range and L range under consideration ranges from around 30 – 200 min. This is much faster than the sampling time of one-half CRRES orbit (5.5 hours) and cannot be resolved in our data. On this long timescale, particles and boundary always track each other.

5. Storm Time Ion Composition

The main feature of the ionospheric origin ions (O^+ and He^+) is the strong similarity in the data when compared to protons H^+, which have their source in the plasma sheet. As outlined in section 4, the dawnside delay in the appearance of protons during the storm main phase is a convection drift effect from a plasma sheet source region: The fact that the ionospheric heavy ions show this same effect and have such similar dynamics points strongly to the same immediate source for these ions, the plasma sheet.

While the direct access of these ionospheric ions into the ring current seems to be from the plasma sheet, there is no doubt that the origin of these ions is the ionosphere. There must therefore be a preceeding mechanism which transports these ions out of the polar ionosphere downtail along open field lines, from where they convect down into the plasma sheet and from there undergo the same plasma sheet dynamics as those of any other ion. The data from CRRES do not have the time resolution or the spatial coverage to examine this process.

There has been much discussion on the role of direct access of ionospheric ions from the auroral zone, being accelerated along field-aligned potentials and then scattered at the inner edge of the plasma sheet near $L = 7$. As these ions from these origins appear together with the ions from the plasmaspheric regions, it is normally impossible to distinguish the two mechanisms.

During the dawn storm in Plate 1 we see a small flux increase in O^+ (Plot 4 and 5), He^{++} (plot 6 and 7), and H^+ (plot 10 and 11) during the main phase. The main phase is covered by two CRRES half orbits, and the observed slight flux increase seems to move inward from one half orbit to the next. This movement is well correlated with a dawn-dusk electric field that penetrates progressively earthward during this time (plot 3). Given that the main body of freshly injected ions arrives at dawn only during the recovery phase (see section 4 for details), where does this population come from? The timing and position of the first sign of this slight enhancement (dotted line in Plate 1) are consistent with an auroral acceleration source, but the energy of the ions is well beyond that which can be produced by field-aligned potentials in the auroral zone. We suggest that the source of this population is the previously trapped ions below $L = 7$ that remain trapped even under disturbed conditions (inside the red dotted line in Plate 5), which are convected deep into the inner magnetosphere by the large convection field exisiting during onset. It is only at dawn that this separate process becomes observable during the main phase, since access of new plasma sheet ions is restricted at dawn.

The He^{++} ions are coming from the solar wind and may have direct access into the magnetosphere during the main phase of the storm. Their intensity is directly related to the composition of the solar wind driver and can vary greatly from storm to storm.

He^+ is a charge exchange product of He^{++} and reaches its strongest intensity a few days later. He^+ does also have an ionospheric source, as its main dynamics are similar to those of the other ionospheric ion species. Namely, the peak of the He^+ is near the peak of the other ion species, which is $\sim 1\ R_E$ farther inward compared to He^{++}. We suggest that He^+ comes primarily from an ionospheric source via normal plasma sheet dynamics and is later increased further by addition of the charge exchange products from He^{++}, which explains the delayed peak intensity in the storm recovery phase.

We have thus shown that the ionospheric contribution to the storms occurs mainly by way of the plasma sheet and that direct injection from the ionosphere to the ring current does not play a role at the energies observed here. There is a small contribution of previously trapped ions to ring current regions which is minor.

Cold ionospheric ions are drawn out at high latitudes and enter the plasma sheet downtail owing to the dawn-dusk electric field on open field lines (polar cap potential). Subsequently the ions are energized and convected toward the Earth together with the existing plasma sheet population. *Baker et al.* [1996] showed that for realistically large convection electric fields one can expect most ionospheric ions to drift into the plasma sheet relatively close to the Earth, on the timescale of hours. A quantitative question remains: Is the existing reservoir of ionospheric ions in the plasma sheet sufficient to provide the source of the storm-injected ring current ions, or is a much enhanced ionospheric outflow required during storm onset to create a sufficiently large source? These questions are beyond the scope of this paper.

6. Summary

The investigations of the particle and field measurements during these three storms have lead to the following results:

1. The plasma sheet has been identified as the source of the ring current ions.
2. During the main phase, plasma sheet ions have access to all MLTs except to dawn for ions >30 keV.

3. A partial ring current exists at higher energies during storm onset, this leads to an asymmetric ring current during this phase.
4. With the beginning of the recovery phase the main body of the ring current is on closed drift paths, and symmetry is restored.
5. For the ring current energies observed here there is no direct ionospheric access to the ring current ($\sim>$ 30 keV).
6. There is some evidence for an inner magnetospheric ion source in the form of the previously trapped population, which is minor compared to newly convected ions from the plasma sheet, this minor contribution is only observable at dawn during storm onset.

In contrast to the common view, plasma sheet ions in the energy range from 5 to 28 keV contribute significantly in the energy density of the ring current during the storm main phase. They are convected into the inner magnetosphere owing to the strong cross-tail electric fields and are the main current carriers during this stage affecting D_{st}. During the main phase the D_{st} is dominated by these energies, which are still on open drift paths which are highly unsymmetric.

In the recovery phase the prime contribution to the ring current is now on closed, symmetric drift paths, and the asymmetric portion of the convection pattern has moved to higher L and thus plays a minor role. The ground-based observations of *Grafe* [1999] which point to a persistent, quiet time, small asymmetry of the ring current are consistent with this interpretation.

In the debate on the significance and origin of other ion species during storms we have shown that the main source of ring current heavy ions is the same as that for protons, and that they follow the same dynamics as those from the plasma sheet. The unique configuration of drift paths and Alfven layers at the dawnside has allowed us to identify an inner magnetospheric source of ionospheric ions during the main phase and has shown that this is a minor contribution only.

CRRES particle and field data in a L versus time format allows tracking of the full storm time dynamics in a consistent way. Magnetic field data, observed at different magnetic local times, show large stretching of the magnetic field lines down to L values below $L = 4$. The stretching or flattening of the magnetic field is here also observed at dawn and dusk, showing this to be a truly global effect [*Korth and Vampola*, 1994; *Mouikis et al.*, 1998]. The B_Z component of the magnetic field minus the Olson-Pfitzer model is depressed over the whole measured L range at the beginning of the main phase. With the beginning of the storm recovery phase a well-developed ring current (dark blue line at L values between 3 and 5) is observed. The location of this depression correlates well with the ring current ions.

An enhanced dawn-dusk convection electric field is observed during the main phase of the storm and vanishes during the recovery of the storm. The penetration depth of the convection electric field to low L values depends on the size of the magnetic storm and is directly related to the access depth of plasma sheet particles during the main phase. Trapping occurs rapidly when the field vanishes, an effect which is very clear in the data presented here.

Acknowledgments.

We thank A. Grafe (at the GeoforschungsZentrum Potsdam), D. Rowland (at Univ. of Minnesota, Minneapolis), H. J. Singer (at NOAA, Boulder), and T. Cayton (at LANL, Los Alamos) for many useful discussions.

Janet G. Luhman thanks the referees for their assistance in evaluating this paper.

References

Baker, D. N., T. I. Pulkinnen, P. Toivanen, M. Hesse, and R. McPherron, A possible interpretation of cold ion beams in the Earth's tail lobe, *J. Geomagn.*, *48*, 699–710, 1996.

Borovsky, J. E., M. F. Thomsen, D. J. McComas, T. E. Cayton, and D. J. Knipp, Magnetospheric dynamics and mass flow during the November 1993 storm, *J. Geophys. Res.*, *103*, 26,373–26,394, 1998.

Carpenter, D. L., B. L. Giles, C. R. Chappell, P. M. E. Décréau, R. R. Anderson, A. M. Persoon, A. J. Smith, Y. Corcuff, and P. Canu, Plasmasphere dynamics in the duskside bulge region: A new look at an old topic, *J. Geophys. Res.*, *98*, 19,243–19,271, 1993.

Daglis, I. A., The role of magnetosphere-ionosphere coupling in magnetic storm dynamics, in *Magnetic Storms, Geophys. Monog.*, edited by B. T. Tsurutani et al., vol. 98, pp. 107–116, AGU, Washington, D.C., 1997.

Elphic, R., L. A. Weiss, M. F. Thomsen, D. J. McComas, and M. B. Moldwin, Evolution of plasmaspheric ions at geosynchronous orbit during times of high geomagnetic activity, *Geophys. Res. Lett.*, *23*, 2189–2192, 1996.

Friedel, R. H. W., and A. Korth, Long-term observations of keV ion and electron variability in the outer radiation belt from CRRES, *Geophys. Res. Lett.*, *22*, 1853–1856, 1995.

Gonzalez, W. D., J. A. Joselyn, Y. Kamide, H. W. Kroehl, G. Rostoker, B. T. Tsurutani, and V. M. Vasyliunas, What is a geomagnetic storm?, *J. Geophys. Res.*, *99*, 5771–5792, 1994.

Grafe, A., Are our ideas about dst correct?, *Ann. Geophys.*, *17*, 1–10, 1999.

Grebowsky, J. M., Time-dependent plasmapause motion, *J. Geophys. Res.*, *76*, 6193–6197, 1971.

Gussenhoven, M. S., D. A. Hardy, and W. J. Burke, DMSP/F2 electron observations of equatorward auroral boundaries and their relationship to magnetospheric electric fields, *J. Geophys. Res.*, *86*, 768–778, 1981.

Gussenhoven, M. S., D. A. Hardy, and N. Heinemann, Systematics of the equatorward diffuse auroral boundary, *J. Geophys. Res.*, *88*, 5692–5708, 1983.

Hardy, D. A., D. M. Walton, A. D. Johnstone, M. F. Smith, M. P. Gough, A. Huber, J. Pantazis, and R. Burkhardt, Low energy plasma analyzer, *IEEE Trans. Nucl. Sci,*, *40*, 246–251, 1993.

Jordan, C. E., J. N. Bass, M. S. Gussenhoven, H. J. Singer, and R. V. Hilmer, Comparison of magnetospheric magnetic field models with CRRES observations during the August 26, 1990, storm, *J. Geophys. Res.*, *97*, 16,907–16,919, 1992.

Kawasaki, K., and S.-I. Akasofu, Low-latitude DS component of geomagnetic storm field, *J. Geophys. Res.*, *76*, 2396–2405, 1971.

Korth, A., and R. H. W. Friedel, Dynamics of energetic ions and electrons between $L = 2.5$ and $L = 7$ during magnetic storms, *J. Geophys. Res.*, *102*, 14,113–14,122, 1997.

Korth, A., and A. L. Vampola, Cross-L motion of a relativistic electron belt formed in the slot region, *J. Geophys. Res.*, *99*, 13,529–13,535, 1994.

Korth, A., G. Kremser, B. Wilken, W. Güttler, S. L. Ullaland, and R. Koga, Electron and proton wide-angle spectrometer (EPAS) on the CRRES spacecraft, *J. Spacecr. Rockets*, *29*, 609–614, 1992.

Korth, A., R. H. W. Friedel, C. Mouikis, and J. F. Fennell, Storm/substorm signatures in the outer belt, in *Proceedings of the International Conference on Substorms-4, Lake Hamana, Japan, March 9-13*, edited by S. Kokubun and Y. Kamide, pp. 779–783, Terra Sci., Tokyo, 1998.

Korth, H., M. F. Thomsen, J. E. Borovsky, and D. J. McComas, Plasma sheet access to geosynchronous orbit, *J. Geophys. Res.*, *104*, 25,047–25,061, 1999.

Kurita, K., and M. Hayakawa, Evaluation of the effectiveness of theoretical model calculations in determining the plasmapause structure, *J. Geophys.*, *57*, 130–135, 1985.

Mouikis, C. G., A. Korth, R. H. W. Friedel, and J. F. Fennell, Dawn/dusk dropouts due to storms/substorms near the outer radiation belt: Observations from CRRES, in *Proceedings of the International Conference on Substorms-4, Lake Hamana, Japan, March 9-13*, edited by S. Kokubun and Y. Kamide, pp. 707–710, Terra Sci., Tokyo, 1998.

Olson, W., and K. Pfitzer, Magnetospheric magnetic field modeling, *annual scientific report, AFOSR Contract F44620-75-C-0033, McDonnell Douglas Astronaut. Co., Huntington Beach, Calif.*, 1977.

Rowland, D. E., and J. R. Wygant, Dependence of the large-scale, inner magnetospheric electric field on geomagnetic activity, *J. Geophys. Res.*, *103*, 14,959–14,964, 1998.

Singer, H. J., W. P. Sullivan, P. Anderson, F. Mozer, P. Harvey, J. Wygant, and W. McNeil, Fluxgate magnetometer instrument on CRRES, *J. Spacecr. Rockets*, *29*, 599–600, 1992.

Wilken, B., W. Weiss, D. Hall, M. Grande, F. Soeraas, and J. F. Fennell, Magnetospheric ion composition spectrometer onboard the CRRES spacecraft, *J. Spacecr. Rockets*, *29*, 585–591, 1992.

Williams, D. J., The Earth's ring current: Present situation and future thrusts, *Phys. Scr.*, *T18*, 140–151, 1987.

Wygant, J., D. Rowland, H. J. Singer, M. Temerin, F. Mozer, and M. K. Hudson, Experimental evidence on the role of the large spatial scale electric field in creating the ring current, *J. Geophys. Res.*, *103*, 29,527–29,544, 1998.

Wygant, J. R., P. R. Harvey, D. Pankow, F. S. Mozer, N. Maynard, H. Singer, M. Smiddy, W. Sullivan, and P. Anderson, CRRES electric field/Langmuir probe instrument, *J. Spacecr. Rockets*, *29*, 601–604, 1992.

J. F. Fennell, The Aerospace Corporation, El Segundo, CA 90009.

R. H. W. Friedel and H. Korth, Los Alamos National Laboratory, Los Alamos, NM 87545.

A. Korth, Max-Planck-Institut für Aeronomie, 37191 Katlenburg-Lindau, Germany.

C. G. Mouikis, Space Science Center, University of New Hampshire, Durham, NH 03824.

J. R. Wygant, School of Physics and Astronomy, University of Minnesota, MN 55455.

Received November 23, 1999; revised February 15, 2000; accepted February 15, 2000.